A&A 625, L10 (2019)
https://doi.org/10.1051/0004-6361/201935656

Astronomy & Astrophysics

LETTER TO THE EDITOR

A geometric distance measurement to the Galactic center black hole with 0.3% uncertainty*

The GRAVITY Collaboration: R. Abuter[8], A. Amorim[6], M. Bauböck[1], J. P. Berger[5], H. Bonnet[8], W. Brandner[3], Y. Clénet[2], V. Coudé du Foresto[2], P. T. de Zeeuw[10,1], J. Dexter[1], G. Duvert[5], A. Eckart[4,13], F. Eisenhauer[1], N. M. Förster Schreiber[1], P. Garcia[7], F. Gao[1], E. Gendron[2], R. Genzel[1,11], O. Gerhard[1], S. Gillessen[1], M. Habibi[1], X. Haubois[9], T. Henning[3], S. Hippler[3], M. Horrobin[4], A. Jiménez-Rosales[1], L. Jocou[5], P. Kervella[2], S. Lacour[2,1], V. Lapeyrère[2], J.-B. Le Bouquin[5], P. Léna[2], T. Ott[1], T. Paumard[2], K. Perraut[5], G. Perrin[2], O. Pfuhl[1], S. Rabien[1], G. Rodriguez Coira[2], G. Rousset[2], S. Scheithauer[3], A. Sternberg[12,14], O. Straub[1], C. Straubmeier[4], E. Sturm[1], L. J. Tacconi[1], F. Vincent[2], S. von Fellenberg[1], I. Waisberg[1], F. Widmann[1], E. Wieprecht[1], E. Wiezorrek[1], J. Woillez[8], and S. Yazici[1,4]

(Affiliations can be found after the references)

Received 10 April 2019 / Accepted 25 April 2019

ABSTRACT

We present a 0.16% precise and 0.27% accurate determination of R_0, the distance to the Galactic center. Our measurement uses the star S2 on its 16-year orbit around the massive black hole Sgr A* that we followed astrometrically and spectroscopically for 27 years. Since 2017, we added near-infrared interferometry with the VLTI beam combiner GRAVITY, yielding a direct measurement of the separation vector between S2 and Sgr A* with an accuracy as good as 20 μas in the best cases. S2 passed the pericenter of its highly eccentric orbit in May 2018, and we followed the passage with dense sampling throughout the year. Together with our spectroscopy, in the best cases with an error of 7 km s^{-1}, this yields a geometric distance estimate of $R_0 = 8178 \pm 13_{\rm stat.} \pm 22_{\rm sys.}$ pc. This work updates our previous publication, in which we reported the first detection of the gravitational redshift in the S2 data. The redshift term is now detected with a significance level of 20σ with $f_{\rm redshift} = 1.04 \pm 0.05$.

Key words. black hole physics – astrometry – Galaxy: nucleus

1. Introduction

Measuring distances is a key challenge in astronomy. While many distance estimators rely on secondary calibration methods, the basis for the whole distance ladder is laid by a few methods. These methods all compare an angular scale on sky with a size that is known in absolute terms. Foremost is of course the parallax method. It compares an observed reflex motion on the sky, measured in angular units with the size of Earth's orbit. Recently, *Gaia* improved the number and quality of available parallaxes substantially (Gaia Collaboration 2018). However, *Gaia* works in the optical and at moderate spatial resolution and does not provide any parallaxes toward the crowded and highly dust-obscured center of the Milky Way. The extinction can be overcome by observing at longer wavelengths, in the near-infrared (NIR; 1−5 μm). Very large telescopes with adaptive optics (AO), and recently, interferometry between large telescopes (Gravity Collaboration 2017), overcome the stellar crowding. This allowed us to determine the orbits of 40 stars around the central massive black hole with periods between 13 and a few thousand years (Gillessen et al. 2017). These stars offer another direct method of determining a distance. The distance to the Galactic center (GC), R_0, can be determined by comparing the radial velocities (measured in km/s) of these stars with their proper motions (measured in mas/yr). The measurement is direct because this can be done for individual stellar orbits, as opposed to using a sample of stars together with a dynamical model like in van de Ven et al. (2006) for the globular cluster ω Cen or in Chatzopoulos et al. (2015) for the Milky Way nuclear cluster.

Most suitable for the orbit method is the star S2 on a 16-year orbit (the second shortest period known so far, Meyer et al. 2012), with a semimajor axis $a \approx 125$ mas. S2 has an apparent K-band magnitude of $m_K \approx 14$, which is bright enough for spectroscopy. It is a massive, young main-sequence B star (Ghez et al. 2003; Martins et al. 2008; Habibi et al. 2017) that offers a few atmospheric absorption lines in the observable parts of the spectrum. Several works used S2 to measure the distance to the GC. The first measurement was in Eisenhauer et al. (2003), who reported $R_0 = 7940 \pm 420$ pc. Eisenhauer et al. (2005) updated this value to $R_0 = 7620 \pm 320$ pc. Ghez et al. (2008) reported $R_0 = 8400 \pm 400$ pc, and Gillessen et al. (2009) differed slightly with $R_0 = 8330 \pm 350$ pc. More recently, Boehle et al. (2016) measured $R_0 = 7860 \pm 140 \pm 40$ pc, and Gillessen et al. (2017) obtained $R_0 = 8320 \pm 70 \pm 140$ pc. Here and in what follows, the first error is statistical, and the second error is systematic. All these measurements rely on AO data. For

* GRAVITY has been developed by a collaboration of the Max Planck Institute for Extraterrestrial Physics, LESIA of Paris Observatory/CNRS/UPMC/Univ. Paris Diderot and IPAG of Université Grenoble Alpes/CNRS, the Max Planck Institute for Astronomy, the University of Cologne, the Centro de Astrofísica e Gravitaçâo, and the European Southern Observatory.

general recent overviews of R_0 determinations, see Genzel et al. (2010) and Bland-Hawthorn & Gerhard (2016).

The star S2 passed the pericenter of its orbit in May 2018, an event that we followed in detail with astrometry and spectroscopy (Gravity Collaboration 2018a). The primary goal of these observational efforts was the detection of relativistic effects in the orbital motion. However, the data also allow for an unprecedentedly accurate measurement of R_0 because of the large swing in radial velocity (from +4000 to $-2000\,\mathrm{km\,s^{-1}}$) and the large orbital phase that was covered in 2018. Gravity Collaboration (2018a) presented the detection of the gravitational redshift from Sgr A* in the S2 spectra. Our previous analysis included data up to end of June 2018. It addressed the question whether the gravitational redshift and Doppler terms are in agreement with the predictions of Einstein's theory of relativity. At the same time, our orbital solution also included the most precise determination of R_0 so far, $R_0 = 8122 \pm 31\,\mathrm{pc}$, where the error is only statistical. Several authors studying the Milky Way structure have used this result (McGaugh 2018; Drimmel & Poggio 2018; Mróz et al. 2019; Eilers et al. 2019). Here, we update our value for R_0, using data up to the end of 2018, and we apply the relativistic corrections assuming General Relativity is correct. This yields one fit parameter less. We also investigate the systematic error on R_0 from our measurement, which we did not consider in Gravity Collaboration (2018a).

2. Data

Gravity Collaboration (2018a) used 45 AO-based astrometric points (after down-sampling), 77 radial velocities, and 30 GRAVITY interferometric data points. The present study adds ten epochs of radial velocity measurements from late June 2018 to late September 2018, and ten epochs of GRAVITY astrometry. Furthermore, we reanalyzed our radial velocity data from SINFONI and the GRAVITY astrometry, implementing an improved understanding of the respective systematic effects. This also led to a slightly different data selection and different grouping of the observations.

For the SINFONI data we revisited the wavelength calibration, yielding an improved wavelength dispersion solution. Where possible, we determined the radial velocities by template fitting. The uncertainties are a combination of formal fit error, wavelength error, and the error introduced by selecting a certain extraction mask in the field of the integral field unit. For the details see Appendix A.

For the GRAVITY data we replaced the manual frame selection with an objective outlier-rejection and included the (minor) effect of atmospheric differential refraction. The data analysis includes data selection, binary fitting, correction for atmospheric refraction, outlier rejection, nightly averaging, correction for effective wavelength, adding systematic errors, and error scaling. We report the details in Appendix B.

Overall, our new data set consists of 169 AO-based astrometry points between 1992 and 2019, 91 radial velocities between 2000 and 2019, and 41 GRAVITY-based astrometry points in 2017 and 2018.

Our AO data set samples the on-sky motion of S2 at high cadence. The distance between subsequent data points is typically smaller than the size of the point spread function. Any confusion event with unrecognized faint stars thus might affect several data points, leading to correlated measurements. As in Gravity Collaboration (2018a), we therefore down-sampled the AO data set into intervals of constant arc length on the sky, and we down-weighted these AO data by a factor two in order to take the additional uncertainty due to unseen confusion events into account. Furthermore, we omitted the 2018 data where additional confusion with Sgr A* affects the data, leading to 48 AO-based astrometric data points. We also developed a different approach for the same problem, namely a noise model (see Sect. 3). This gives a second data set, in which we used all 169 AO-based astrometric points.

3. Analysis

We used the same techniques as in Gravity Collaboration (2018a) and Gillessen et al. (2017). The analysis essentially consists of one step: determining the best-fit orbit for the data given, and the corresponding uncertainties. We employed a χ^2-minimization to determine the best-fit, and for the uncertainties, we used the standard error matrix approach, a Markov chain Monte Carlo (MCMC) sampler and a bootstrapping technique. The latter bootstraps an artificial data set by drawing from the original data separately for the AO astrometry, the radial velocities, and the GRAVITY data. In order to avoid problems that might arise because the AO points are correlated, we used the down-sampled data set for the bootstrapping.

For a different approach with the AO data, we implemented a noise model of the type presented in Plewa & Sari (2018) for the AO-based astrometry. Such a model has the advantage that it estimates the additional amount of error and the correlation length from the data themselves, avoiding any prior choices on how to treat the data. In our implementation, we exchanged the temporal correlation length of Plewa & Sari (2018) with a spatial one. The underlying reason for a correlation between different data points is confusion with unseen stars that can be described naturally by a length scale in the image plane. Because S2 has a widely varying proper motion, a temporal correlation length is less suited. This model adds two additional fit parameters: the spatial correlation length and the typical confusion amplitude, which correspond to the down-sampling and down-weighting in the other data set. We did not exclude all 2018 data for this data set, but only the epochs at which Sgr A* apparently affected the position measurements, as visible in an elongated source structure or excess flux of S2. We also analyzed a third data set excluding all AO astrometry. Perhaps somewhat surprisingly, the two years of GRAVITY data already are the much stronger constraint for the orbit compared to the past 27 years of AO imaging data.

Compared to the analysis in Gravity Collaboration (2018a), we included in the calculation of the transverse Doppler effect the apparent proper motion of Sgr A* to the southwest of $(-3.151, -5.547)\,\mathrm{mas\,yr^{-1}}$, a reflex of the solar motion around the Milky Way center (Reid & Brunthaler 2004). This corresponds to $v_\odot \approx 250\,\mathrm{km\,s^{-1}}$, while S2 at pericenter reaches an on-sky motion of $v_{S2} \approx 7320\,\mathrm{km\,s^{-1}}$. Because in the Doppler formula a term of type $(v_{S2} + v_\odot)^2 \approx v_{S2}^2(1 + 2v_\odot/v_{S2})$ occurs, the proper motion of Sgr A* leads to a small but noticeable correction. We parameterized the strength of the combined redshift and transverse Doppler effect with an artificial parameter f_redshift such that $f_\mathrm{redshift} = 0$ corresponds to classical physics, while $f_\mathrm{redshift} = 1$ corresponds to the effects occurring as predicted by General Relativity. Including the proper motion of Sgr A* induces a change of $\Delta f_\mathrm{redshift} = +0.038$, and a change in distance of $\Delta R_0 = +6\,\mathrm{pc}$.

4. Results

4.1. Distance R_0 to the Galactic center

If the fit has as few free parameters as possible, the estimate for R_0 is the most precise. We therefore assumed that General

Table 1. Best-fit parameters for our three data sets.

Parameter	Down-sampled data	Noise model fit	GRAVITY only
R_0 [pc]	8179 ± 13	8178 ± 13	8175 ± 13
Mass [$10^6\ M_\odot$]	4.154 ± 0.014	4.152 ± 0.014	4.148 ± 0.014
x_0 [mas]	−1.04 ± 0.36	−0.65 ± 0.36	N.A.
y_0 [mas]	−0.47 ± 0.35	−0.73 ± 0.35	N.A.
vx_0 [μas yr^{-1}]	68 ± 31	68 ± 32	N.A.
vy_0 [μas yr^{-1}]	158 ± 31	108 ± 31	N.A.
vz_0 [km s^{-1}]	−3.3 ± 1.5	−3.0 ± 1.5	−2.8 ± 1.5
a [mas]	125.072 ± 0.084	125.066 ± 0.084	125.065 ± 0.086
e	0.884282 ± 0.000064	0.884293 ± 0.000064	0.884288 ± 0.000064
i [°]	133.911 ± 0.052	133.904 ± 0.052	133.883 ± 0.053
Ω [°]	228.067 ± 0.041	228.075 ± 0.041	228.091 ± 0.041
ω [°]	66.250 ± 0.035	66.253 ± 0.035	66.257 ± 0.035
$t_{\rm peri}$ [yr] − 2018	0.3790 ± 0.0014	0.3790 ± 0.0014	0.3789 ± 0.0014
UTC date	19.5.2018 09:53	19.5.2018 09:51	19.5.2018 09:47
red. χ^2	0.82	1.10	1.00

Notes. The parameters x_0, y_0, vx_0, and vy_0 describe the location and motion of the mass in the coordinate system of the AO data in RA and Dec. Because GRAVITY directly measures the separation vector, we do not need to include such coordinate system offsets for the GRAVITY data. The third velocity vz_0 is the offset of the motion in the radial direction along the line of sight, the negative sign means a blueshift or a motion toward the observer. The parameters $(a, e, i, \Omega, \omega, t_{\rm peri})$ are the classical orbital elements semimajor axis, eccentricity, inclination, position angle of ascending node, longitude of pericenter, and the epoch of pericenter passage. The orbital elements are defined as the osculating orbital elements at $t = 2010.0$, i.e., the conversion to position and velocity is done at that epoch assuming a Kepler orbit.

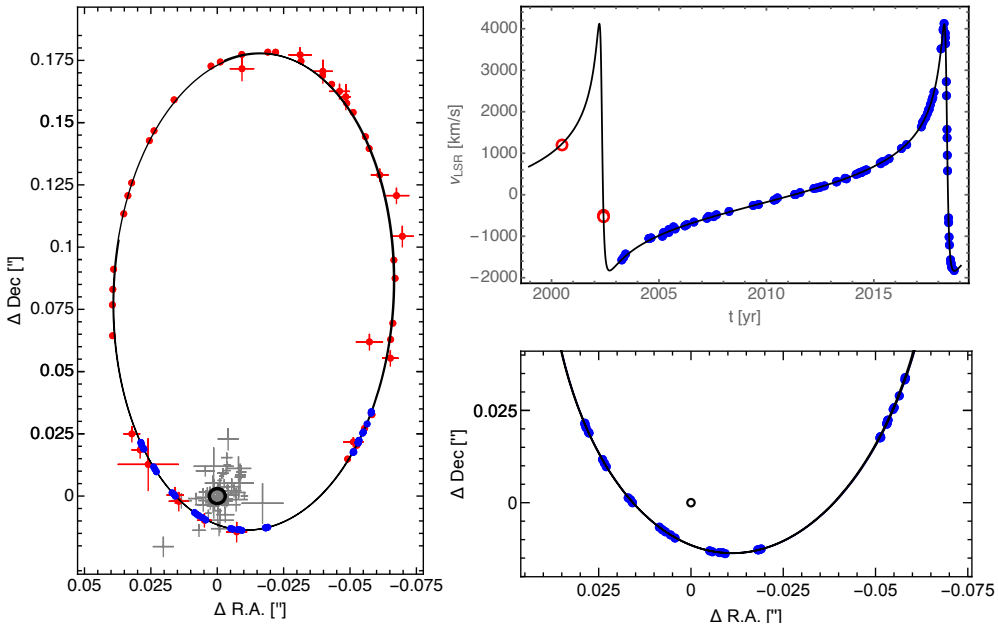

Fig. 1. Orbit of S2. *Left*: on-sky view of the astrometric data (red: AO data, blue: GRAVITY data) in the down-sampled version with the best-fit orbit (black ellipse). The black circle marks the position of Sgr A*. The locations of previous AO-based flares agree with that position (gray crosses). *Right top*: radial velocity data of S2 together with the best-fit orbit. The blue data are from the VLT, the red are earlier epochs from the Keck data set (Ghez et al. 2008). *Right bottom*: zoom into the on-sky orbit in 2017 and 2018, showing the GRAVITY data that have error bars smaller than the symbol size.

Relativity holds and fixed the parameter $f_{\rm redshift} = 1$. We further used the Rømer delay and included the first-order correction from the Schwarzschild metric. The coordinate system parameters only apply to the AO astrometry because GRAVITY directly measures the vector S2 - Sgr A*.

We list our best-fit results in Table 1 and show the best fit in Fig. 1. The error bars we report are the formal fit errors from the error matrix. The three data sets yield completely consistent parameters within the formal uncertainties. The reduced χ^2 values by construction of the errors are close to 1 (Appendices A and B).

The noise model has two additional free parameters, the noise amplitude $\sigma = 0.83 \pm 0.15$ mas and the spatial correlation length $\lambda = 21.2 \pm 3.8$ mas. These numbers define by how much a certain data point is expected to be off from the model, given the other data. The correlation length is on the same order of magnitude as the AO point spread function radius, and the amplitude is reasonable. Our best-fit σ corresponds to a perturbing star of $m_K \approx 17$ at a distance of our best-fit λ (Plewa & Sari 2018).

Using the MCMC sampler, we obtained the full 13-dimensional posterior distribution. All parameters are well

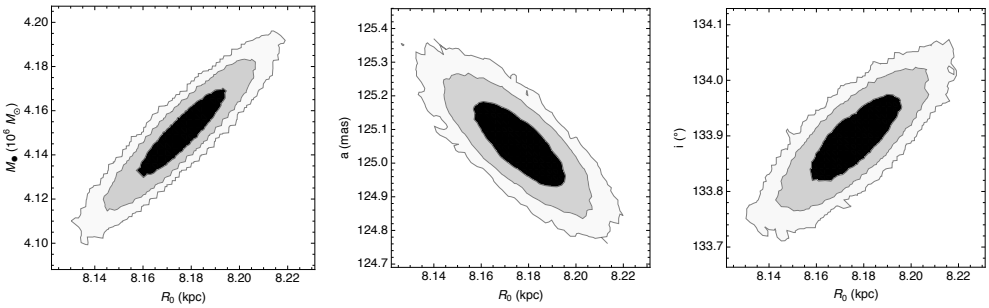

Fig. 2. Selected posterior densities as obtained from the MCMC sampler with $N = 200\,000$, here for the noise model data set. The contour lines mark the 1, 2, and 3σ levels. We only show the diagrams with the strongest correlations. All parameters are well determined (see Appendix D).

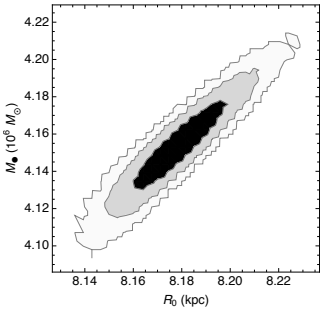

Fig. 3. Posterior distribution for R_0 and mass from our bootstrap sample. The contour lines mark the 1, 2, and 3σ levels.

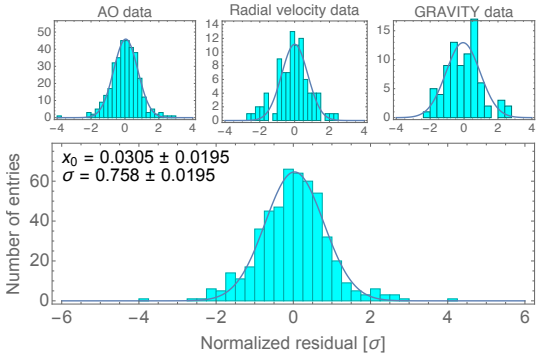

Fig. 4. Histograms of the normalized residuals, the ratio of residual to error for each data point. *Top row*: individually for the three subsets of data. *Bottom*: combined data set.

constrained, and Fig. 2 shows the diagrams with the strongest parameter correlations: mass versus R_0, semimajor axis versus R_0, and inclination versus R_0. The most probable value agrees with the best-fit value, and the 1σ uncertainty from the posterior is 13 pc, which is fully consistent with the estimate from the error matrix. We furthermore estimated our errors by bootstrapping (and refitting each artificial data set). For this, we used the down-sampled data set because here the most important correlation between data points is removed. Figure 3 shows the resulting distribution for $N = 20\,000$ bootstraps. The most likely value agrees with the best-fit value, and so do the error bars: $R_0 = 8178^{+13}_{-12}$ pc.

Figure 4 shows the normalized residual (residual divided by the error) distributions for each of the three subsets of data and for the whole data set. The distributions are well behaved and reasonably close to a Gaussian with mean 0 and width 1.

The size of the R_0 error of $13/8178 \approx 0.16\%$ is comparable to what a simple estimate yields. R_0 is directly related to the ratio of proper motion (arc length divided by time) and radial velocity. The most constraining part of the orbit is the pericenter swing, which we followed with GRAVITY in 2017 and 2018.

- The arc length is ≈150 mas, more than 1000× larger than the median 2D error of the 41 GRAVITY points[1]. The astrometric precision is thus at the 0.01% level and does not contribute significantly to the statistical error.
- The median error of the radial velocity data in 2017 and 2018 is 14.4 km s^{-1}, and we have 35 data points. The mean absolute radial velocity of our data in 2017 and 2018 is 2300 km s^{-1}. The spectroscopic precision is thus at the 0.1% level. It dominates the measurement error, and it is of the same magnitude as the actual statistical error on R_0.

We conclude that $R_0 = 8178 \pm 13_{\rm stat.}$ pc. However, we still lack an estimate for the systematic error.

4.2. Systematic errors

Our estimate for R_0 is direct and as such does not depend on intermediate calibration steps. Any systematic error is directly related to how accurately we understand the instruments we use, that is, how accurate are the on-sky positions we measure and how accurate are the radial velocities. Figure 2 shows the strongest parameter correlations for R_0 from the posterior distribution of the 13-dimensional fit. They are with mass, semimajor axis, and inclination. These correlations can be understood qualitatively.

- R_0 is inversely proportional to the semimajor axis a. A biased determination of a in angular units would bias R_0 because the radial velocity data determine a in absolute units; for S2, $a \approx 1023$ AU. The slope of the correlation in Fig. 2 (middle) confirms this, $R_0 \times a \approx 1023$ AU. The instrumental reason why a could be biased is an error in the image scale. A scale error of 1% would imply a distance error of ≈80 pc.
- The inclination i would be biased if the image scale were off in one dimension only. The MCMC shows a sensitivity of R_0 to i of 3.75°/kpc. At the inclination of S2, the sensitivity of the scale change to a change in i amounts to 1.2%/°.
- Kepler's third law, $GM = 4\pi^2(a \times R_0)^3/P^2$ (where the semimajor axis a is measured in angular units), shows that our mass measurement is equivalent to determining the period P because the nominator $a \times R_0$ is a constant, see above. The MCMC shows a sensitivity of R_0 to M of 1.4×10^3 $M_\odot$ pc^{-1}

[1] The median 1D error of the 2018 GRAVITY data is 60 μas, and for 2017 it is 145 μas. These numbers already take into account the scatter from night to night. The uncertainties for individual data points within a single night are smaller (Gravity Collaboration 2018b). The difference in median error between 2017 and 2018 is caused by the improvement in fiber positioning implemented for 2018. The median error over the whole data set of 41 points is 86 μas 1D, or equivalently, 121 μas 2D.

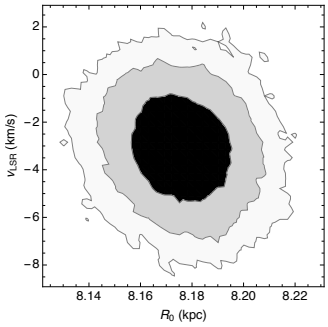

Fig. 5. Posterior distribution for R_0 and the offset in radial velocity. The contour lines mark the 1, 2, and 3σ levels.

at the best-fit R_0, corresponding to $\approx$1 day pc^{-1} for the sensitivity to P. We note that the error we make in measuring the period due to the uncertainty in the underlying data is captured in the statistical error on R_0. What matters here would be a systematic error in measuring time, which we can exclude at the relevant level. The mass-distance degeneracy is not a source of potential systematic error.

We conclude that if the parameter degeneracies were to introduce a systematic error on R_0, it would originate from an error in the astrometry. Furthermore, we note that the GRAVITY data completely dominate our astrometry (see Table 1), and that the AO + GRAVITY data sets yield the same result as the GRAVITY-only fit. This means that the uncertainty in the GRAVITY astrometry dominates the systematic error from the astrometry. In Appendix C we show that we estimate this uncertainty to be 19 pc or 0.24%.

When we used the GRAVITY astrometry, we assumed that the near-infrared (NIR) counterpart of Sgr A* is at the position of the center of mass. Gravity Collaboration (2018b) reported that the flaring emission from Sgr A* moves in a circular pattern with a radius of a few Schwarzschild radii, $\approx$50 μas. The flares are compact regions of transiently heated electrons that emit synchrotron light, powered probably by magnetic reconnection events (Dodds-Eden et al. 2009). They occur very close to the innermost stable circular orbit, and orbital motion of a few 10 μas has been proposed since their discovery (Genzel et al. 2003; Broderick & Loeb 2005; Hamaus et al. 2009). Observationally, the center of motion matches the position of the mass to within $\approx$50 μas. We used this as uncertainty on our assumption and estimated the effect on R_0 by artificially displacing the mass by that amount. This yields changes in R_0 of +8 pc, −8 pc, −6 pc, and +5 pc to the north, south, east, and west. We include 6 pc in the systematic error for the assumption that GRAVITY directly measures the separation vector between S2 and mass center.

With full coverage of the orbit, the measurement of R_0 is no longer degenerate with the offset vz_0 in radial velocity (Fig. 5, cf. Ghez et al. 2008). A general offset in the radial velocity would be absorbed fully into vz_0, but it would not affect our measurement of R_0. The zeroth order of the wavelength calibration is thus not a source of systematic error. The leading order could only be the first order, that is, the dispersion solution.

Our spectra are calibrated with a higher order polynomial, using multiple atmospheric lines in the same spectra as calibration points. From the residuals of our dispersion solution at these calibration points, we estimated the systematic uncertainty in the wavelength axis to 2.5 km s^{-1} over the range relevant for S2. Together with the mean absolute radial velocity in 2017 and 2018 (2300 km s^{-1}), we obtain a systematic error of 0.11% or 9 pc.

Taken together, we thus estimate our systematic error on R_0 to be 22 pc. Our main result is

$$R_0 = 8178 \pm 13_{\rm stat.} \pm 22_{\rm sys.}\ {\rm pc}.$$

The statistical error is dominated by the measurement uncertainties of the radial velocities, and the systematic error by the GRAVITY astrometry.

4.3. Update on the gravitational redshift in S2

With the new data sets in hand, we repeated the posterior analysis of Gravity Collaboration (2018a) to determine the combined effect of gravitational redshift and transverse Doppler effect. Using an orbit model including the first-order correction due to the Schwarzschild metric and including the Rømer delay, we find $f_{\rm redshift} = 1.047 \pm 0.052$ for the noise model fit and $f_{\rm redshift} = 1.036 \pm 0.052$ when we use the down-sampled data set. Figure 6 shows the radial velocity residuals to the classical part of the true best-fit orbit. For this we set $f_{\rm redshift} = 0$ without refitting after fitting with $f_{\rm redshift} = 1$. We compared these residuals to the true model (i.e., with the effects turned on, $f_{\rm redshift} = 1$). We exclude that purely Newtonian physics can describe our data at a significance level of 20σ.

4.4. Distance estimate without radial velocities

Our GRAVITY measurement also provides the first direct distance measurement from orbital motion without the need for radial velocities. The key for this is the Rømer effect: The light travel time across the orbit causes astrometric points to appear slightly ahead or lagging behind the orbit, depending on whether S2 is in front of or behind Sgr A*. For a Keplerian orbit with astrometric data only and no light-time travel effect, the distance cannot be determined. The best-fit mass and distance are degenerate along a line $M \propto R_0^3$. Because the light travel time across the orbit between 2017 and 2018 (where we have GRAVITY data) is about three days and because we can detect the daily motion of S2 in the GRAVITY data, our astrometry breaks the degeneracy. Figure 7 (left) shows that this is indeed the case. The best-fit distance for this case is $R_0 = 9.5 \pm 1.5$ kpc, consistent with our best estimate. To our knowledge, Anglada-Escudé & Torra (2006) were the first to propose this type of distance measurement, but we are not aware of an application anywhere so far.

If we were to ignore the Rømer effect for the purely astrometric data set, we would not obtain as a return a fully degenerate mass-distance relation. Instead, the fit then tries to become as small a distance as possible (Fig. 7, right), that is, in the sense of a limit, we obtain $R_0 \to 0$. This is where the light travel time effect is minimal, as imposed by the wrong orbit model without Rømer delay. This just shows in a different way that our astrometry requires a finite speed of light and thus can estimate R_0.

5. Discussion

The best estimate for R_0 from Bland-Hawthorn & Gerhard (2016) using only their set of ten independent best measurements that did not invoke Sgr A* is $R_0 = 8210 \pm 80$ pc, in perfect agreement with our value. This means that Sgr A* is indeed at the center of the Milky Way bulge.

Our value of R_0 together with the proper motion of Sgr A* of 6.379 ± 0.026 mas yr^{-1} $= 30.24 \pm 0.12$ km s^{-1} kpc^{-1} from Reid & Brunthaler (2004) implies $\Theta_0 + V_\odot = 247.4 \pm 1.4$ km s^{-1}, where Θ_0 is the rotation speed of the local standard of rest (LSR)

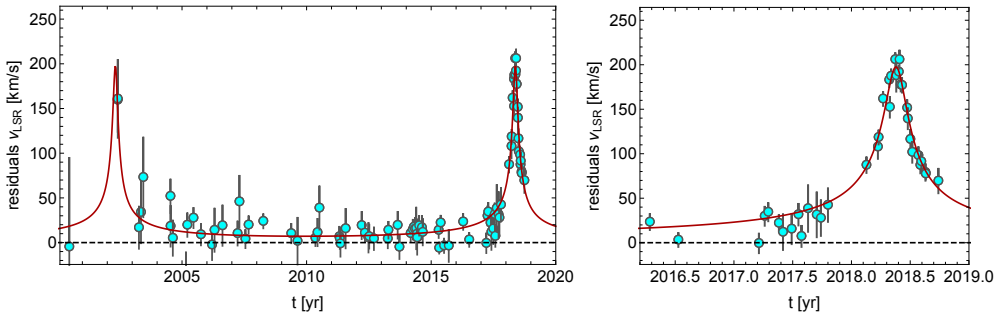

Fig. 6. Update of the posterior analysis of Gravity Collaboration (2018a). The panels show the residuals of the radial velocity data to the best-fit orbit in which post-fit the redshift and transverse Doppler effect were turned off (line at 0, $f_{\rm redshift} = 0$). The 2018 data show a highly significant excursion. The red line gives the orbit with $f_{\rm redshift} = 1$. General relativity is an excellent description for the residuals.

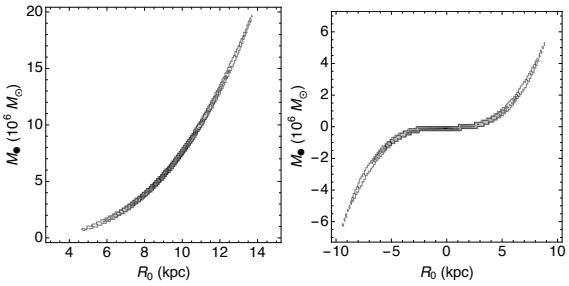

Fig. 7. Posterior distributions for the data set without radial velocities. *Left*: using the correct orbit model. *Right*: using an orbit model that neglects the Rømer effect. In this plot we allowed negative distances (and correspondingly negative masses) to avoid having a bound of the parameter space at 0, where the actual maximum of the distribution falls.

and $V_\odot$ is the peculiar solar motion toward $l = 90°$. The error on $\Theta_0 + V_\odot$ is composed roughly equally of the error in the proper motion of Sgr A* and the uncertainty in R_0. This constraint on $\Theta_0 + V_\odot$ is compatible with the recent determination from Hayes et al. (2018), who found $\Theta_0 + V_\odot = 253 \pm 6\,{\rm km\,s^{-1}}$ from *Gaia* astrometry of the Sgr stream.

Bland-Hawthorn & Gerhard (2016) estimate $V_\odot = 11 \pm 2\,{\rm km\,s^{-1}}$, but to take into account the radial variations in the median v_ϕ seen by Gaia Collaboration (2018), we used a total uncertainty of $4\,{\rm km\,s^{-1}}$. Together with our estimate for $\Theta_0 + V_\odot$ this implies $\Theta_0 = 236.9 \pm 4.2\,{\rm km\,s^{-1}}$. From combining *Gaia* DR2 and APOGEE data, Eilers et al. (2019) found $\Theta_0 = 229 \pm 6\,{\rm km\,s^{-1}}$, where the error is the reported systematic uncertainty. Wegg et al. (2019) used *Gaia* DR2 and RR Lyrae stars to derive $\Theta_0 = 217 \pm 6\,{\rm km\,s^{-1}}$. Using trigonometric parallaxes of high-mass star-forming regions, Reid et al. (2014) find $\Theta_0 = 240 \pm 8\,{\rm km\,s^{-1}}$.

Another remarkable result is the fact that the offset in the radial velocity, vz_0, is small and consistent with zero. The offset absorbs any possible systematic offset in the radial velocity.

- The surface gravity of S2 contributes $\Delta vz_0 = GM_{S2}/r_{S2}c = 1.6\,{\rm km\,s^{-1}}$ (Lindegren & Dravins 2003), where we used r_{S2}, the radius of S2, and M_{S2}, its mass, from Habibi et al. (2017).
- The contribution of the Galactic potential can be approximated by $\Delta vz_0 = v_\odot^2/c\,\ln(R_0/R_{S2})$, where $v_\odot$ is the Sun's circular galactocentric speed and R_{S2} is the galactocentric radius of S2 (Lindegren & Dravins 2003). The approximation surely does not hold inside the sphere of influence of Sgr A* (≈3 pc), where the massive black hole dominates the potential. However, because of the logarithm in the expression, the actual effective value for R_{S2} does not matter strongly. With $v_\odot \approx 230\,{\rm km\,s^{-1}}$ and $R_{S2} = 3$ pc, we obtain $\Delta vz_0 = 1.4\,{\rm km\,s^{-1}}$, and when we use the apocenter distance $R_{S2} = 0.009$ pc, the number is $\Delta vz_0 = 2.4\,{\rm km\,s^{-1}}$.
- Frame-dragging by a maximally spinning black hole might contribute an average $\lesssim 0.2\,{\rm km\,s^{-1}}$ to the redshift (Angélil et al. 2010; Grould et al. 2017).
- Light bending and Shapiro delay reach $\lesssim 4\,{\rm km\,s^{-1}}$ (Angélil et al. 2010) but are highly peaked around pericenter and flip sign, so that they do not induce a bias on vz_0.
- Contributions from the solar system are around $3\,{\rm m\,s^{-1}}$, and thus negligible.

A similarly sized offset in vz_0 might arise from the uncertainty of the construction of the LSR, which by its original definition should not include a motion component in the radial direction, $U_{\rm LSR} = 0$. The LSR correction applied to our data uses the values from Schönrich et al. (2010), who reported $U_\odot = 11.10^{+0.69}_{-0.75}\,{\rm km\,s^{-1}}$, where $U_\odot$ is the solar motion in the direction of the GC. In their review, Bland-Hawthorn & Gerhard (2016) concluded that this was $U_\odot = 10.0 \pm 1.0\,{\rm km\,s^{-1}}$. The variations in the median radial velocity of stars measured by Gaia Collaboration (2018) in the nearby disk suggest that $U_{\rm LSR}$ is uncertain on the scale of several km/s.

Furthermore, an offset in vz_0 could be due to the intrinsic motion of Sgr A* with respect to the Milky Way. Reid & Brunthaler (2004) measured the motion of Sgr A* perpendicular to the Galactic plane to be $0.4 \pm 0.9\,{\rm km\,s^{-1}}$. For the third dimension, the motion along the Galactic plane, Reid et al. (2009) reported $-7.2 \pm 8.5\,{\rm km\,s^{-1}}$, and the update in Reid et al. (2014) implies tighter constraints around $2{-}3\,{\rm km\,s^{-1}}$. The expected "Brownian motion" of Sgr A* that is due to scattering with stars in its vicinity is even slightly smaller than these limits with $0.2\,{\rm km\,s^{-1}}$ (Chatterjee et al. 2002; Merritt et al. 2007).

The parameter vz_0 is the sum of these offsets. Our fit results and the two redshift terms yield a value of $\approx -6 \pm 6\,{\rm km\,s^{-1}}$. The uncertainty on this number is larger than the fit error because of the systematic uncertainties, such as the actual value for the Galactic potential that is used for S2, but also the systematic uncertainties in the wavelength calibration. The most likely reason why the sum is small is that the summands are small. Under this hypothesis, we conclude that to within a few km/s, Sgr A* is at rest at the center of the Milky Way and that the LSR is moving tangentially. The value is lower than might be expected from the combined effect of Galactic bar and spiral arms; however, their quantitative effect on the velocity streamlines at the solar position is not well known.

Our data very strongly constrain the angular diameter of Sgr A*. Because mass and R_0 are correlated, the constraint is stronger than what simple error propagation would yield. We find $R_S/R_0 = 10.022 \pm 0.020_{\rm stat.} \pm 0.032|_{\rm sys.}\,\mu$as. The combined uncertainty corresponds to 50 000 km at our R_0. This sets a strong prior for the analysis of data obtained from global millimeter very long baseline interferometry that aims at resolving Sgr A* (Falcke et al. 2000; Doeleman et al. 2009).

A potential caveat of our analysis might be that the physical model of the orbit is too simple. So far, S2 did not reveal any signs of binarity. For GRAVITY, S2 is an unresolved point source (Gravity Collaboration 2017). The resolution of GRAVITY in GC observations is about 2.2 mas × 4.7 mas, excluding a source extension larger than or a companion farther away than ≈1 mas. Chu et al. (2018) used the radial velocity data of S2 and reported an upper limit of $M_{\rm companion} \sin i \leq 1.6\,M_\odot$ for periods between 1 and 150 days. Longer periods would not be stable against tidal break-up. Furthermore, the motion of either S2 or Sgr A* could be affected by as yet unknown massive objects in the GC. To some extent, such a perturbation can always be absorbed into the orbital elements (Gualandris et al. 2010), resulting in biased estimates for the parameters. According to our current knowledge, S2 is a suitable probe for R_0. It is an ordinary massive main-sequence star of type B0-B3 (Ghez et al. 2003; Martins et al. 2008; Habibi et al. 2017). The atmospheric absorption lines we used are expected to be fair tracers of the motion of the star, together with its (unresolved) photocenter.

The value from Boehle et al. (2016), $R_0 = 7.86 \pm 0.14 \pm 0.04$ kpc, disagrees with our result. However, it comes from a combined fit of the stars S2 and S38. The S2-only result of these authors is $R_0 = 8.02 \pm 0.36 \pm 0.04$ kpc, which is completely consistent with our result. Furthermore, we note that combining different stars in the orbit fit tends to change the parameter mass and R_0 by rather large amounts (Gillessen et al. 2017) because small inconsistencies in the data sets are amplified by the fact that in the mass-R_0 plane two narrow, curved posterior distributions are combined. The statistical error of a combined fit does not catch this and could thus miss part of the true uncertainties.

Overall, we used accurate radial velocities from SINFONI and proper motions from GRAVITY of the star S2 as it orbits Sgr A* to set the absolute size of the orbit and determine the distance to the GC with unprecedented accuracy to $R_0 = 8178$ pc. The statistical error is only 13 pc and is dominated by the measurement errors of the radial velocities. The systematic error of 22 pc is dominated by the calibration uncertainties of the astrometry. Our analysis also demonstrates that the relative velocity of the LSR along the line of sight to Sgr A* is consistent with zero to within a few km/s, implying that Sgr A* is at rest in the GC and the LSR is moving tangentially. The addition of further SINFONI and GRAVITY data taken in 2018 also allowed us to increase the significance of the previously published measurement of the gravitational redshift caused by Sgr A* to 20σ.

Acknowledgements. We are very grateful to our funding agencies (MPG, ERC, CNRS, DFG, BMBF, Paris Observatory, Observatoire des Sciences de l'Univers de Grenoble, and the Fundação para a Ciência e Tecnologia), to ESO and the ESO/Paranal staff, and to the many scientific and technical staff members in our institutions who helped to make NACO, SINFONI, and GRAVITY a reality. S.G. acknowledges support from ERC starting grant No. 306311 (PROGRESO). F.E. and O.P. acknowledge support from ERC synergy grant No. 610058 (BlackHoleCam). J.D., M.B., and A.J.-R. were supported by a Sofja Kovalevskaja award from the Alexander von Humboldt foundation. A.A. and P.G. acknowledge support from FCT-Portugal with reference UID/FIS/00099/2013.

References

Angélil, R., Saha, P., & Merritt, D. 2010, ApJ, 720, 1303
Anglada-Escudé, G., & Torra, J. 2006, A&A, 449, 1281
Bland-Hawthorn, J., & Gerhard, O. 2016, ARA&A, 54, 529
Boehle, A., Ghez, A. M., Schödel, R., et al. 2016, ApJ, 830, 17
Broderick, A. E., & Loeb, A. 2005, MNRAS, 363, 353
Chatterjee, P., Hernquist, L., & Loeb, A. 2002, ApJ, 572, 371
Chatzopoulos, S., Fritz, T. K., Gerhard, O., et al. 2015, MNRAS, 447, 952
Chu, D. S., Do, T., Hees, A., et al. 2018, ApJ, 854, 12
Dodds-Eden, K., Porquet, D., Trap, G., et al. 2009, ApJ, 698, 676
Doeleman, S., Agol, E., & Backer, D. 2009, Astro2010: The Astronomy and Astrophysics Decadal Survey [arXiv:0906.3899]
Drimmel, R., & Poggio, E. 2018, Res. Notes Am. Astron. Soc., 2, 210
Eilers, A.-C., Hogg, D. W., Rix, H.-W., & Ness, M. K. 2019, ApJ, 871, 120
Eisenhauer, F., Schödel, R., Genzel, R., et al. 2003, ApJ, 597, L121
Eisenhauer, F., Genzel, R., Alexander, T., et al. 2005, ApJ, 628, 246
Falcke, H., Melia, F., & Agol, E. 2000, ApJ, 528, L13
Fritz, T. K., Gillessen, S., Trippe, S., et al. 2010, MNRAS, 401, 1177
Gaia Collaboration (Katz, D., et al.) 2018, A&A, 616, A11
Genzel, R., Schödel, R., Ott, T., et al. 2003, Nature, 425, 934
Genzel, R., Eisenhauer, F., & Gillessen, S. 2010, Rev. Mod. Phys., 82, 3121
Ghez, A., Duchêne, G., Matthews, K., et al. 2003, ApJ, 586, L127
Ghez, A., Salim, S., Weinberg, N. N., et al. 2008, ApJ, 689, 1044
Gillessen, S., Eisenhauer, F., Trippe, S., et al. 2009, ApJ, 692, 1075
Gillessen, S., Plewa, P. M., Eisenhauer, F., et al. 2017, ApJ, 837, 30
Gravity Collaboration (Abuter, R., et al.) 2017, A&A, 602, A94
Gravity Collaboration (Abuter, R., et al.) 2018a, A&A, 615, L15
Gravity Collaboration (Abuter, R., et al.) 2018b, A&A, 618, L10
Grould, M., Vincent, F. H., Paumard, T., & Perrin, G. 2017, A&A, 608, A60
Gualandris, A., Gillessen, S., & Merritt, D. 2010, MNRAS, 409, 1146
Habibi, M., Gillessen, S., Martins, F., et al. 2017, ApJ, 847, 120
Hamaus, N., Paumard, T., Müller, T., et al. 2009, ApJ, 692, 902
Hayes, C. R., Law, D. R., & Majewski, S. R. 2018, ApJ, 867, L20
Lacour, S., Eisenhauer, F., Gillessen, S., et al. 2014, A&A, 567, A75
Lindegren, L., & Dravins, D. 2003, A&A, 401, 1185
Martins, F., Gillessen, S., Eisenhauer, F., et al. 2008, ApJ, 672, L119
McGaugh, S. S. 2018, Res. Notes Am. Astron. Soc., 2, 156
Merritt, D., Berczik, P., & Laun, F. 2007, AJ, 133, 553
Meyer, L., Ghez, A., Schödel, R., et al. 2012, Science, 338, 84
Mróz, P., Udalski, A., Skowron, D. M., et al. 2019, ApJ, 870, L10
Perrin, G., & Woillez, J. 2019, A&A, 625, A48
Plewa, P. M., & Sari, R. 2018, MNRAS, 476, 4372
Reid, M. J., & Brunthaler, A. 2004, ApJ, 616, 872
Reid, M. J., Menten, K. M., Zheng, X. W., et al. 2009, ApJ, 700, 137
Reid, M. J., Menten, K. M., Brunthaler, A., et al. 2014, ApJ, 783, 130
Rousselot, P., Lidman, C., Cuby, J.-G., Moreels, G., & Monnet, G. 2000, A&A, 354, 1134
Schönrich, R., Binney, J., & Dehnen, W. 2010, MNRAS, 403, 1829
van de Ven, G., van den Bosch, R. C. E., Verolme, E. K., & de Zeeuw, P. T. 2006, A&A, 445, 513
Wegg, C., Gerhard, O., & Bieth, M. 2019, MNRAS, 485, 3296
Witzel, G., Martinez, G., Hora, J., et al. 2018, ApJ, 863, 15
Woillez, J., & Lacour, S. 2013, ApJ, 764, 109

[1] Max Planck Institute for Extraterrestrial Physics (MPE), Giessenbachstr. 1, 85748 Garching, Germany
e-mail: ste@mpe.mpg.de
[2] LESIA, Observatoire de Paris, PSL Research University, CNRS, Sorbonne Universités, UPMC Univ. Paris 06, Univ. Paris Diderot, Sorbonne Paris Cité, 92195 Meudon Cedex, France
[3] Max-Planck-Institute for Astronomy, Königstuhl 17, 69117 Heidelberg, Germany
[4] 1. Physikalisches Institut, Universität zu Köln, Zülpicher Str. 77, 50937 Köln, Germany
[5] Univ. Grenoble Alpes, CNRS, IPAG, 38000 Grenoble, France
[6] CENTRA and Universidade de Lisboa – Faculdade de Ciências, Campo Grande, 1749-016 Lisboa, Portugal
[7] CENTRA and Universidade do Porto – Faculdade de Engenharia, 4200-465 Porto, Portugal
[8] European Southern Observatory, Karl-Schwarzschild-Str. 2, 85748 Garching, Germany
[9] European Southern Observatory, Casilla, 19001 Santiago 19, Chile
[10] Sterrewacht Leiden, Leiden University, Postbus 9513, 2300 RA Leiden, The Netherlands
[11] Departments of Physics and Astronomy, Le Conte Hall, University of California, Berkeley, CA 94720, USA
[12] School of Physics and Astronomy, Tel Aviv University, Tel Aviv 69978, Israel
[13] Max-Planck-Institute for Radio Astronomy, Auf dem Hügel 69, 53121 Bonn, Germany
[14] Center for Computational Astrophysics, Flatiron Institute, 162 5th Ave., New York, NY 10010, USA

Appendix A: Radial velocities from SINFONI

For the SINFONI data we improved the wavelength calibration. Explicitly, we modified our atmospheric line list that serves as reference for the wavelength calibration by excluding double lines or lines with a low signal-to-noise ratio (S/N) following the line atlas of Rousselot et al. (2000). We also improved the fine-tuning of the spectrum to the OH lines, leading to an improved wavelength dispersion solution. With these changes, we typically achieved a calibration error of below 2 km s^{-1}, measured by the residuals of the OH lines. With the improved data reduction, we re-reduced all available data since October 2004. The earlier data (two epochs in 2004 and one in 2003) were obtained during commissioning time and need a dedicated calibration procedure, which we did not repeat. We combined data from different nights when the expected velocity change was smaller than the calibration error. We omitted one measurement from 2008 with low S/N (from a single ten-minute exposure) and included one more epoch from 2009 and 2015 each and two more from 2010 and 2011 each. We split up data that previously were combined into one cube into two epochs in two occasions, in 2013 and 2015.

For spectra in which both the He-I line (2.112 μm) and Brackett-γ (2.166 μm) lines are unaffected by atmospheric residuals, we used template fitting to determine the radial velocities. For this we fit the long-time average S2 spectrum (Habibi et al. 2017) to the data. For spectra with sufficient S/N and no artifacts (e.g., from imperfect atmosphere correction), template fitting yields more accurate velocities. When either of the lines showed artifacts, we fit a double-Voigt profile to the other unaffected line.

The errors are a combination of fit error and wavelength calibration uncertainty. The fit error is obtained from the formal fit error σ, the S/N, and by varying the pixel selection. For the S/N-related error we established a relation between σ and S/N of $\sigma \propto S/N^{-0.92}$. The 1 / *S/N* behavior is consistent with the uncertainty of a centroid fit (Fritz et al. 2010). To assess the impact of different background subtractions and extraction regions, we extracted eight spectra for each observation and determined the standard deviation of the radial velocities from the different masks. Because these three error estimates are strongly correlated, we used the largest of the three as fit error. We linearly added the wavelength calibration error to obtain a preliminary error. These preliminary errors establish the relative weight of the different radial velocities. Using these, we obtained a preliminary orbit fit, which showed that we overestimated the errors because the residuals around the best preliminary fit are on average 76.8% of the errors. Thus we rescaled the errors by that factor.

With this improvement of the SINFONI analysis, we reach an error of $\approx$7 km s^{-1} for the best data. The median error is 12.3 km s^{-1}, which is an improvement by 46% compared to the previous set of radial velocity data.

Appendix B: Astrometry from GRAVITY data

B.1. Data selection

We started from all observations of Sgr A* or S2 (793 exposures, each 30 × 10s = 5 min on source, i.e., a total of 66 h on source), regardless of observing conditions and instrument performance.

In 2017, S2 was still at a distance of 54−67 mas from Sgr A*, which is comparable to the photometric field of view ($FWHM \approx$ 65 mas), and too little flux from Sgr A* was injected into the fibres of the exposure pointing on S2 for a reliable interferometric binary signature (Perrin & Woillez 2019). We therefore only considered the observations centered on Sgr A* (261 exposures). We furthermore rejected all Sgr A* observations for which the instrument internal pupil control (Gravity Collaboration 2017) reported an error >6 cm for any of the telescopes (12 exposures) or for which the pointing of any telescope was too far from Sgr A* (83 exposures). We used a box spanning ΔRA = $-45 \ldots 10$ mas, ΔDec = $-30 \ldots 30$ mas around Sgr A*, which especially avoided pointings toward the opposite side of S2. This selection keeps 166 exposures in 2017.

For 2018, we had 373 exposures on Sgr A*. Again, we rejected exposures with pupil errors >6 cm (18 exposures). Because of a newly introduced laser-metrology guiding with substantially improved pointing accuracy, we rejected exposures already when the estimated pointing error for any telescope was outside ΔRA/ΔDec = $-10 \ldots 10$ mas around Sgr A* (35 frames). Because S2 was always closer than 23 mas to Sgr A* during our March–June 2018 observing campaigns, both sources were well within the photometric field of view. We also used the 43 exposures centered on S2 that were obtained during this period. Out of these observations, we rejected three exposures because of a pupil error > 6 cm, and five exposures because of a pointing error larger ΔRA/ΔDec = $-10 \ldots 10$ mas. This yields a total of 355 exposures in 2018.

B.2. Binary fitting and correction for atmospheric refraction

In a second step, three independent subgroups fit the individual exposures with a binary model as described in Gravity Collaboration (2018a,b), using three different codes ("Waisberg (W)", "Pfuhl (P)", "Rodriguez-Coira (R)"). The codes differ in detail in the relative weighting of closure-phases, visibilities, and square visibilities, the free fit parameters (e.g., color of Sgr A* or flux ratio per telescope), and the numerical implementation (e.g., least-squares minimization or MCMC), but give overall consistent results for the binary separations.

We furthermore corrected each binary fit for the differential atmospheric refraction between the comparably "blue" S2 and "red" Sgr A* (see Appendix A7.4 of Gravity Collaboration 2018b). Because Sgr A* was in its faint quiescent state for most of our observations, we used the redder low-flux spectral index $S_\upsilon \propto \upsilon^{-1.6}$ from Witzel et al. (2018) for the subsequent analysis. With $S_\upsilon \propto \upsilon^2$ for S2, and for the given effective spectral resolution of 127 nm (low-resolution mode of GRAVITY), the difference in effective wavelength between S2 and Sgr A* is $\Delta\lambda$ = 2.2 nm, and the resulting atmospheric differential refraction is $\Delta R = 45\,\mu\text{as nm}^{-1} \times \Delta\lambda \tan z = 99\,\mu\text{as} \tan z$, where z is the zenith distance. Because we typically observed the GC close to zenith, the atmospheric differential refraction was on average only 30 μas, and often with opposite signs during a night, which resulted in a mean correction of ΔRA = $-1\,\mu$as and ΔDec = $-5\,\mu$as.

B.3. Outlier rejection and nightly averaging

For each of the three sets of binary fits we determined a preliminary orbit for error scaling and outlier rejection. We rejected observations for which the residuals were outside the 80% quantile constructed in the 2D error-normalized position residual plane[2]. The final data set contains 818 (W), 795 (P), and 737 (R)

[2] The 80% quantile area was constructed using the Mathematica-based quantile regression package https://raw.githubusercontent.com/antononcube/MathematicaForPrediction/master/QuantileRegression.m, Version 1.1, written by Anton Antonov.

binary fits, corresponding to about 400 exposures of five minutes each, that is, about 33 h on source. We combined these and derived nightly (error-weighted) mean and standard errors (with variance weights). Only in the few cases when we had fewer than ten binary-fits per night (26/27 March 2017, 28/29 March 2017, 10/11/12 July 2017) did we combine several nights to one average. The statistical 1D astrometric error of these combined nightly averages is between 10 and 110 μas.

B.4. Correction for effective wavelength, systematic error, and final error scaling

In a last step we corrected the nightly average separation for the effective wavelength shift of 2.3 nm (0.1%) between the wavelength calibration with our 2800 K calibration lamp and the very red highly dust obscured S2/Sgr A* data (see Appendix A7.2 in Gravity Collaboration 2018b).

To account for the systematic error in the wavelength calibration, which we estimate to be 1/20 detector pixel, or equivalently, 2.5 nm, we added in square the corresponding scale error of 0.11%. This error in the effective wavelength translated into an astrometric error of about 10 μas for the time around peri-passage, and up to ΔRA = 66 μas and ΔDec = 33 μas for March 2017, when the S2-Sgr A* distance was largest in our observations.

Finally, to account for unknown additional errors, we scaled the GRAVITY astrometric errors by a factor 2.2 to match the residuals of a best-fitting preliminary orbit. The resulting astrometric errors around the S2 peri-passage in our data from 24 April to 27 June 2018 are ΔRA = 22−101 μas and ΔDec = 38−112 μas, with a mean of 51 μas and 60 μas, respectively.

Appendix C: Systematic error of the GRAVITY astrometry

We obtained the GRAVITY astrometry in the single-field mode. S2 and Sgr A* were close enough in 2017 and 2018 to be fed into the interferometer by a single fiber, the acceptance aperture of which was matched to the telescope point spread function of ≈65 mas. The two sources appear as an interferometric binary to GRAVITY, which means that none of the more complex dual-beam aspects of the instrument (Gravity Collaboration 2017) enter the measurement. The standard equation of interferometric astrometry $\Delta\mathrm{OPD} = \boldsymbol{s} \times \boldsymbol{B}$ sets the effective image scale, where $\boldsymbol{B}$ is the baseline and $\boldsymbol{s}$ is the separation vector that is to be measured. The accuracy of the interferometric baselines and how well we can measure the OPD thus set the accuracy of $\boldsymbol{s}$.

The value for the baseline length to use is the so-called "imaging baseline" in the sense of Woillez & Lacour (2013) and Lacour et al. (2014). The telescope position is then defined by the photocenter of the entrance pupil plane appodized by the fiber mode in the pupil plane. While the telescope geometry is known to the millimeter level, the active mirrors controlling the fiber mode to pupil overlap are more critical and actually limit the baseline accuracy. A systematic error occurs from how well the fiber mode is aligned with the reference point of the pupil tracker. A vignetting of the pupil would also bias the baselines. For an error estimate we used the stability of the pupil position, assuming that the alignment uncertainties overall are at that level. It amounts to 4 cm in the primary mirror space. For the mean baseline length of 81.2 m, an error of 4 cm corresponds to 0.05% or 4 pc on R_0.

The wavelength accuracy of the effective wavelengths sets the accuracy of the OPD. From the standard calibrations of GRAVITY, we estimate that the wavelength accuracy of the interferogram pixels is 0.11% or 9 pc on R_0. This is owing to the faintness of S2 (for interferometric standards), which dictates that we need to observe S2 in low-resolution mode with $R \approx 22$, which corresponds to a wavelength sampling of 50 nm pixel^{-1}.

When the results from the three subgroups and fitting codes are analyzed separately, the standard deviation in the best estimate R_0 is 16 pc. This takes care of the uncertainty in the binary model fit to the GRAVITY data. The difference between the objective outlier rejection and the manual frame selection of Gravity Collaboration (2018a) results in a difference in R_0 of 15 pc. For this estimate, we carried forward the analysis of Gravity Collaboration (2018a) with the new data up to the end of 2018 and included the atmospheric refraction effects. This error, however, is not independent of the error from the fitting by subgroups, and we include the larger of the two (16 pc).

The color difference of S2 and Sgr A* is not known very well, and we include the difference in R_0 determined with and without correction of the atmospheric differential dispersion in our error. It amounts to 5 pc. Adding the different contributions in quadrature, we conclude that the total systematic error on the astrometry is 19 pc, which corresponds to 0.24%.

Appendix D: Full posterior density

In Fig. D.1 we show the full set of posterior densities as obtained from the MCMC sampler with $N = 200\,000$ for the down-sampled data set. All parameters are well determined.

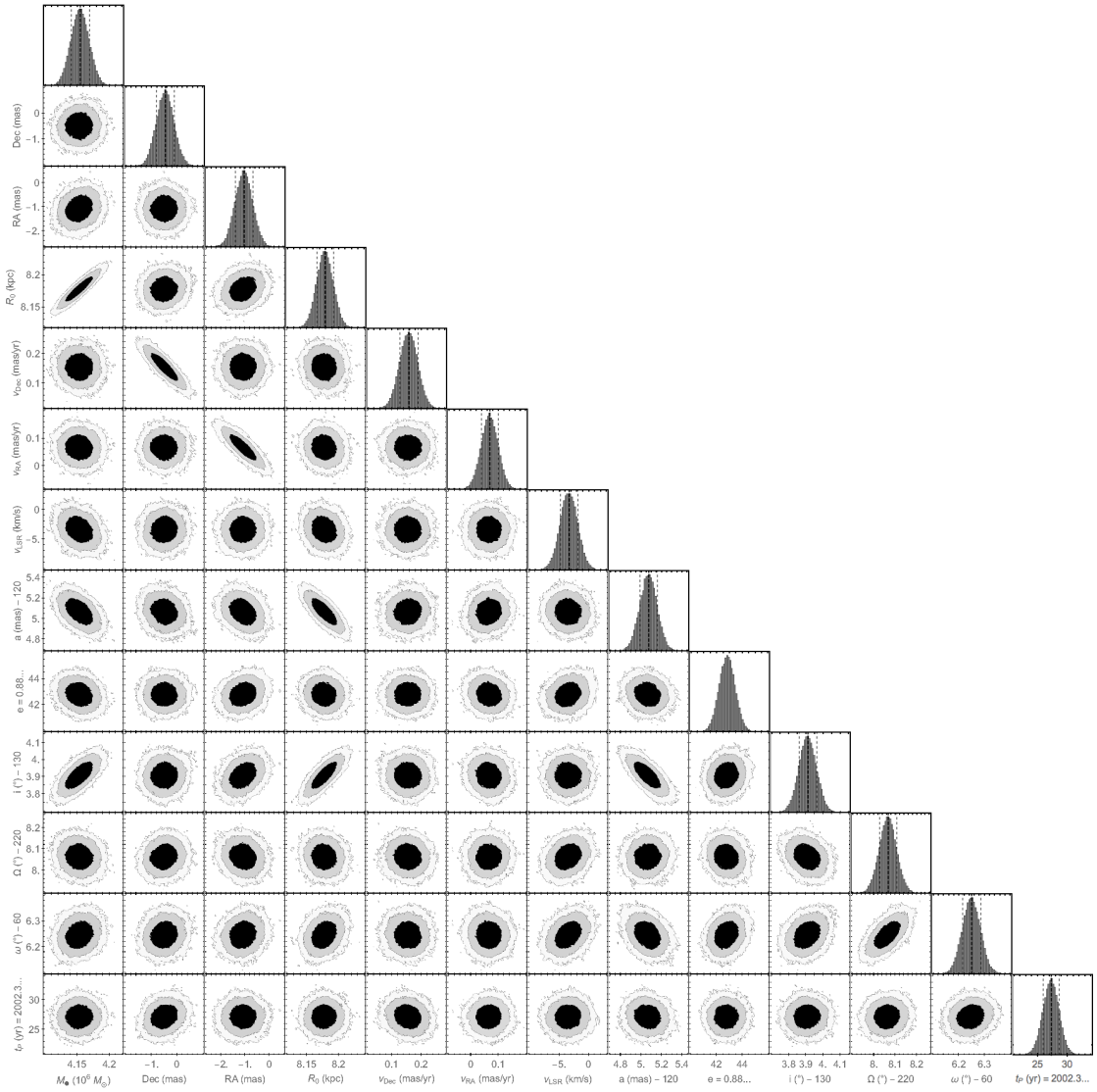

Fig. D.1. Full set of posterior densities as obtained from the MCMC sampler with $N = 200\,000$, here for the down-sampled data set. The contour lines mark the 1, 2, and 3σ levels.